

Flow Assisted Corrosion of API 5L X-70 in Sour Brine induced by Pipe Flow Changes in a Jet Impingement Chamber

A. S. Galván-Luis¹, M. A. Domínguez-Aguilar², J. L. González-Velázquez¹, M. Díaz-Cruz^{1,*},
A. Cervantes-Tobón¹, B. Castro-Domínguez³

¹ Instituto Politécnico Nacional, Departamento de Ingeniería Metalúrgica, IPN-ESIQIE, U.P. Adolfo López Mateos, Zacatenco, C.P. 07738, México, D.F., México.

² Instituto Mexicano del Petróleo, Laboratorio de Producción de Hidrocarburos y Control de la Corrosión, Eje Central Norte Lázaro Cárdenas 152, Col. San Bartolo Atepehuacan, C.P. 07730, México D.F., México.

³ Worcester Polytechnic Institute, Center for Inorganic Membrane Studies, Department of Chemical Engineering, Worcester Massachusetts, WA 01609, US.

*E-mail: mdiazc@ipn.mx

Received: 27 February 2015 / Accepted: 2 October 2015 / Published: 4 November 2015

The corrosion behavior of API 5L X-70 pipe steel was studied in a jet impingement chamber, which simulated the effect of flow rate and contact angle on pipe accessories. Experiments were carried out in sour brine with kerosene and corrosion rates were determined by linear polarization resistance. Corrosion products were characterized by scanning electron microscopy and X-ray diffraction to identify crystalline phases on surface. Parameters under study included flow rate (1.05, 2.36 m/s) and contact angles (30°, 60°, 90°). Highest flow rates were associated to top corrosion rates due to corrosion product detachment on which prevailed that of oxide type, whilst moderate flow rate and static conditions led to a larger number of phases on which sulfides predominated over oxides.

Keywords: Flow assisted corrosion, jet impingement, API 5L X-70 steel.

1. INTRODUCTION

Flow assisted corrosion, also called flow accelerated corrosion (FAC), is related to the metal loss caused by an electrochemical dissolution process of the protective film followed by the release of metallic ions when the metal surface is subjected to a single or two phase flow [1,2]. FAC is a process whereby the normally protective oxide layer on carbon or low-alloy steel is dissolved into a stream of water or water-steam mixtures. The oxide layer becomes thinner and less protective, and the corrosion rate increases. Eventually a steady state is reached when the corrosion and dissolution rates are equal

so stable corrosion rates are maintained. In some areas, oxide layer may be so thin as to expose an apparently bare metal surface. More commonly, however, the corroded surface exhibits a black color commonly identified as magnetite [3]. Damage caused by flow-accelerated corrosion can be characterized as a general reduction of wall thickness rather than a local attack, such as pitting or cracking.

Several studies [4-6] have demonstrated that FAC is increasingly important because of the damage caused to power, nuclear and fossil plants as well as pipeline transmission systems. Metallic failures owed to FAC have derived in a large number of fatalities along with the great cost involved in corrective maintenance and replacements due to plant shutdowns and loss of production. Likewise, FAC has caused catastrophic accidents derived from thickness reduction in the oil & gas pipeline systems, as flow conditions affect mass transfer and remove corrosion products, which adversely reduce its ability to contain fluid pressure.

Flow transmission in pipeline involve complex flow patterns dependent on operational conditions, fluid nature and topography that give rise to shear stresses and corrosion so pipe configuration is an important feature to study. Changes in directions occurring in elbows, bends and expansion curves seems to be the venues where serious damage occurred. Flow incidence and rate along with the shear stress level and general corrosion as thickness thinning can be characterized by changing jet impingement angles. Such studies may be valuable in the material selection process after determining flow conditions and spotting susceptible areas to FAC so as to provide design parameters to help in corrosion rate control. This study aimed to provide some insight into the corrosion mechanism in acidic saline environment under turbulent flow. As corrosion rate is highly dependent on flow mass rate and material film composition, methodical characterization might provide a basis to suggest design parameters, such as top flow rate for several fluids and construction material combinations with minor impairment to equipment and pipes for process and auxiliary services in system engineering [7,8].

In this paper, FAC was studied in carbon steel samples; testing was carried out in a jet impingement chamber, previously design and built in transparent material, provided with a movable plate, where samples can be placed at variable impact angles to simulate changes in flow direction in pipe accessories and pieces of equipment. Coupons of pipe steel API 5L X-70 were subjected to a sour brine flow at different angles of incidence (30° , 60° , 90°) under jet flow conditions of 8 L/min (1.05 m/s) and 18 L/min (2.36 m/s) as testing parameters. Corrosion rates were determined by linear polarization resistance for the flows and angles noted on several sets of three-sample mountings. Likewise, deposited corrosion products were characterized by scanning electron microscopy (SEM) and X-Ray diffraction (XRD) to provide nature of crystalline phases and dependency on the experimental parameters.

2. EXPERIMENTAL PROCEDURE

2.1 Materials and equipment

Carbon steel API 5L-X70 samples were taken from pipe steel, coupons were cut and machined with dimensions of 1 cm x 0.5 cm x 1 cm providing a working area of 0.5 cm². Three samples of

similar dimensions were wet abraded and corner softened before resin mounting; isolated electric wire was welded to each metallic coupons to complete circuit for electrical connection to electrochemical equipment. Coupons were fitted into the impingement chamber to avoid any displacement and cables to move out from chamber.

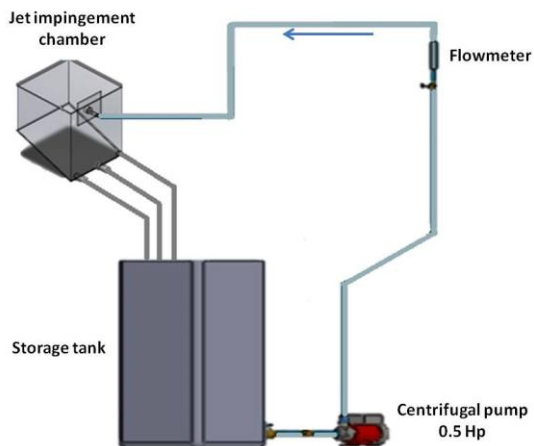


Figure 1. Schematic diagram of the experimental setup.

The experimental equipment used in this investigation is shown in Figure 1, it consists of a test chamber in clear acrylic 5 mm thick. This was made to recirculate a medium consisting of brine prepared according to the NACE standard 1D-196 [9], which was stored in a polyethylene tank with capacity of 100 L. Flow rate was controlled by the adjustment of a rotameter device. The impingement chamber exit consisted of three hoses, which are connected to assist the drain located in the middle of the tank. The equipment pieces used in the present research are shown in more detail below.

2.1.1 Jet impingement chamber

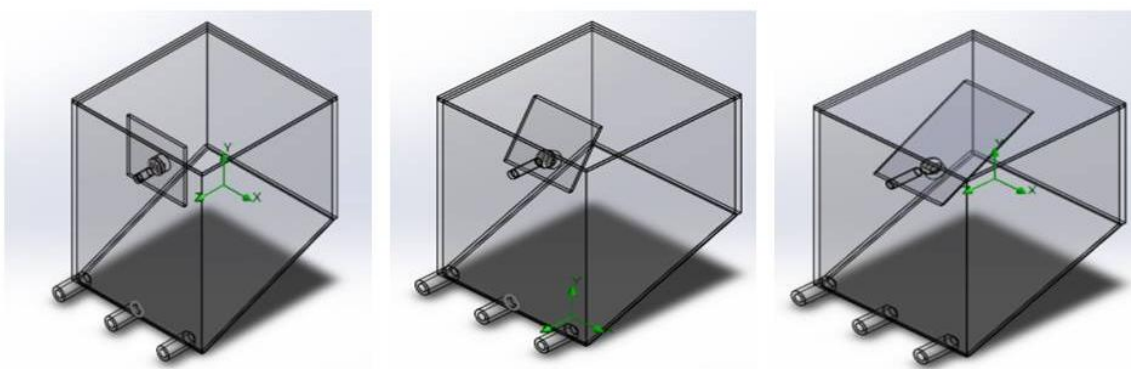


Figure 2. Geometry generated by Solidworks software for the 3 impingement angles on use.



Figure 3. Test chamber in acrylic material.

To carry out the experiment, the geometry of the jet impingement chamber or strike plate chamber, was developed by using Solid Works software program (Fig. 2). The test chamber, whose design is shown in Figure 3, consisted of an empty space of 14-liter capacity with a tilted plate at the bottom for rapid fluid drainage.

Figure 4 shows the inlet and outlet connections as well as the movable plate. It displays the assembly of the striking plate in the test chamber where metallic coupons were placed at impingement angles of 30° , 60° and 90° ; these were selected from evaluations carried out on short and long size elbows from fluid mechanics information. Fluid is fed opposite to the entrance and into the front plate at the middle section to be recirculated from the storage tank to the chamber and from there to the metallic coupon surfaces.



Figure 4. Shock plates positioned at different impingement angles of inclination (a) 30° , (b) 60° and (c) 90° .

2.2. Linear polarization measurements

Linear polarization resistance measurements were performed according to ASTM standards G59 and G102 [10] on previously resin mounted three steel sample electrode for jet impingement tests. The jet impingement chamber, as the electrochemical cell, consisted of an arrangement of three (counter, reference and working) electrodes made of the same material of carbon steel. Experimental

tests were controlled by means of the POWER SUIT commercial software in a potentiostat-galvanostat, Princeton Applied Research model 263A. The polarization scans were performed on steel at ± 20 mV vs. the open circuit potential at a rate of 0.166 mVs^{-1} in a sour brine containing 10% of kerosene and 1383 ppm of H_2S . Corrosion rates were determined from polarization resistance according to Faraday's equation by the available software, as a function of flow rate (8-18 L/min) and testing time (1-8 hours). Three tests were performed every hour after the system stabilized itself at a roughly constant open circuit potential after about 60 minutes to ensure measurement reliability.

2.3. Characterization of corrosion products by SEM and XRD

The surface morphology and composition of the corrosion products formed on the electrode surface were characterized in a JEOL 6300 SEM microscope coupled to EDX detector. X-ray diffraction (XRD) was used to determine the nature of iron phases formed on steel surface of X-70; scanning was performed within the range of 20° to 90° with a step width of 0.02° in a D8 Focus Bruker diffractometer with $\text{Cu K}\alpha$ radiation; further analyses of XRD spectra were carried out with a CreaFit 2.2 DRXW software program.

3. RESULTS AND DISCUSSION

3.1. Chemical analysis and metallography.

The chemical composition (wt. %) of the steel employed in the present study was determined by means an optical emission analysis with a bow and spark spectrometer (BELEC); results are shown in Table 1.

Table 1. Chemical composition of steel API 5L X-70 (wt. %).

C	Mn	Si	P	S	Cr	Cu	Ni	Fe
0.240	1.081	0.284	0.019	0.021	0.156	0.185	0.088	97.926

Microstructure of steel API 5L X-70 was developed by nital etching and it is shown in Figure 5; a dactillar pearlite (dark contrast) along with colonies distributed over a ferrite matrix (light contrast) is observed in a uniform distribution, which is in agreement with carbon steel microstructures obtained by others researchers [11-13].

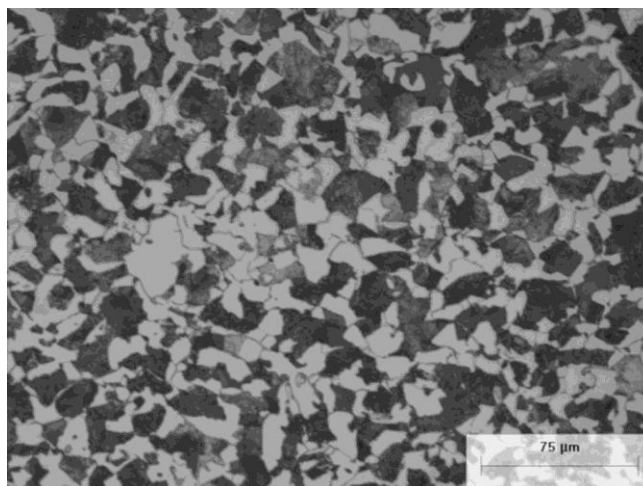


Figure 5. Microstructure of API 5L X-70 steel etched in 5% nital (500X).

3.2 Linear polarization measurements

3.2.1 Corrosion rates as function of inclination angles and flow rate = 8 L/min for steel in sour brine.

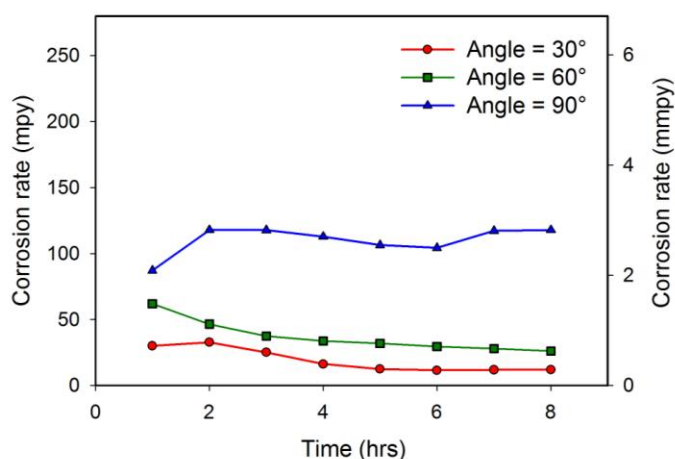


Figure 6. Corrosion rate time dependent after immersion of X-70 in sour brine with kerosene at a flow rate of 8 L/min for impingement angles of 30, 60 and 90°.

Figure 6 shows the corrosion rate as a function of time for the different angles used in this work. At 30° and 60°, the corrosion rate decreased with time though in the case of flow impingement at 90°, the corrosion rate increased above those for 30° and 60°. In the latter, the decrease in corrosion rate was attributed to the persistence of corrosion products, which is more likely because stress seems to be lower. In contrast, at 90° the increase in corrosion rate is derived from the detachment of corrosion products formed due to the flow assisted action in combination with a high impact angle (90°).

3.2.2 Corrosion rates as function of inclination angles and flow rate=18 L/min for steel in sour brine.

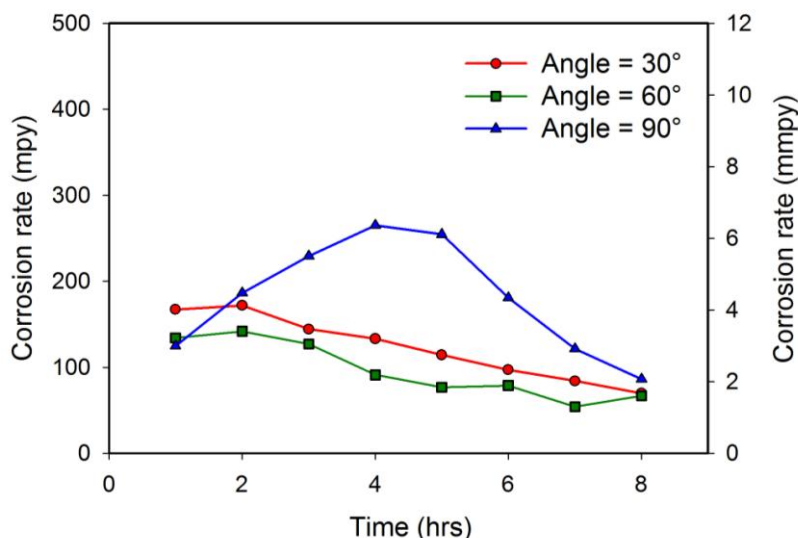


Figure 7. Corrosion rate time dependent after immersion of X-70 in sour brine with kerosene at a flow rate of 18 L/min for impingement angles of 30, 60 and 90°.

In Figure 7, the change in corrosion rate as a function of experimental time for a flow of 18 L/min (2.36 m/s) at 30°, 60° and 90° is observed. Corrosion rate tends to decrease as time is increased; the lowest corrosion rates occurred at an angle of 60°, apparently because the corrosion products formed may seem to be more stable and less soluble. On working at an angle of 90°, the corrosion rate shows a parabolic behavior; where a marked increment in corrosion rate is accompanied by its continuous decrease with time, this decay in corrosion rate was attributed to the continuous formation of corrosion products. At an angle of 90°, the highest initial and final corrosion rates are displayed with 8 L/min, while at 18 L/min only the highest final corrosion rate (Table 2); it appears that the normal stresses developed turns to be higher than those shear stresses formed at lower angles (60-30°), though this matter requires further experimental work. The final corrosion rates might show the apparent higher resistance of corrosion products formed at lower angles (60-30°) due to inherent crystalline phase compositions.

Table 2. Average corrosion rates at the testing conditions

Flow rate	Corrosion rate (mm/y)		Flow rate	Corrosion rate (mm/y)	
8 L/min	V_i	V_f	18 L/min	V_i	V_f
30°	0.76	0.30	30°	4.20	1.77
60°	1.52	0.51	60°	3.42	1.77
90°	2.30	3.04	90°	3.20	2.03

3.3 SEM surface characterization

3.3.1 SEM surface characterization for a flow rate = 8 L/min

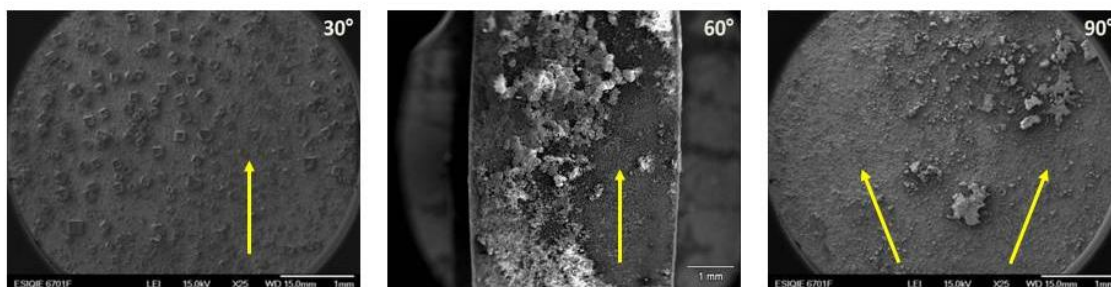


Figure 8. Micrographs of removal of corrosion products at the impingement angles indicated and a flow rate of 8 L/min.

Figure 8 shows the metallic surfaces after testing at the impingement angles indicated. The three surfaces displayed a partial removal of the corrosion products, which provided different patterns as a result of flow and contact angle; removal is presented in a lesser degree on the coupon surface of 30° although it increased as the angle did. The impact direction of flow is indicated by the yellow arrow in each image. The lower removal of corrosion products at 30° is attributed to the presence of NaCl crystals deposited on the surface that may act as a barrier to fluid motion [14], and also to the lower surface resistance to the fluid movement compared to higher inclinations (60, 90°).

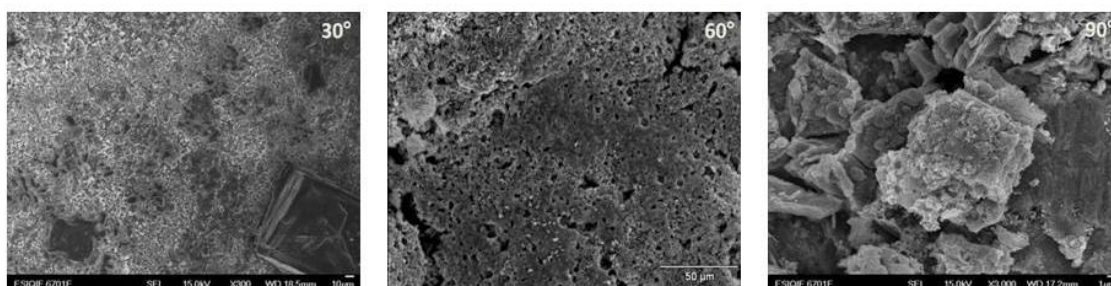


Figure 9. Micrographs of corrosion products deposited on the metallic coupons at the impingement angles indicated and a flow rate of 8 L/min

Figure 9 shows the corrosion products formed on testing, which can be classified as toothed type as it does have an angular shape. On the surfaces, it was observed a first layer called mackinawite and subsequently the growth of other layers consisting of a mixture of oxides and sulfides, and in some cases the presence of sulfate was observed. The relative higher content of corrosion products on the coupon placed at 90° and less on the coupon at 30° might be ascribed to the effect of flow resistance and aeration provided by flow turbulence; this fact may be consistent with the number of phases detected by XRD in Figure 13.

3.3.2 SEM surface characterization for a flow rate = 18 L/min

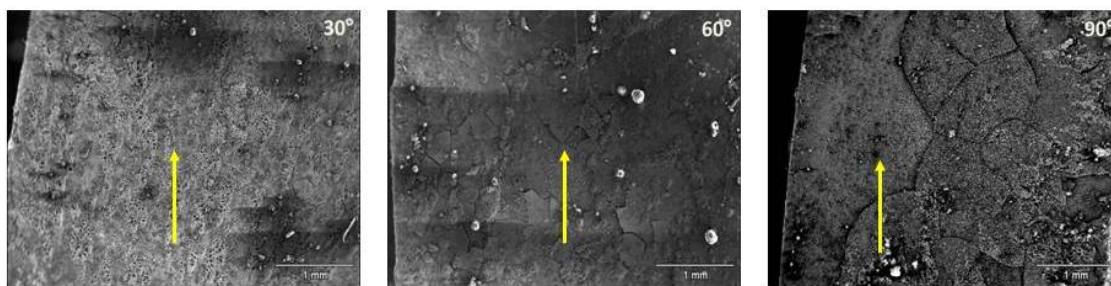


Figure 10. Micrographs of corrosion products deposited on the metallic coupons at the impingement angles indicated and a flow rate of 18 L/min

Figure 10 shows the surfaces of the coupons after conducting the test at a flow rate of 18 L/min (2.36 m/s). It is noticed that flow rate contributed to corrosion product removal and induced cracking in the precursor layer of the formed products. The degree of detachment increased with increasing the angle from 30 to 90°. The flow direction is indicated with arrows in yellow color.

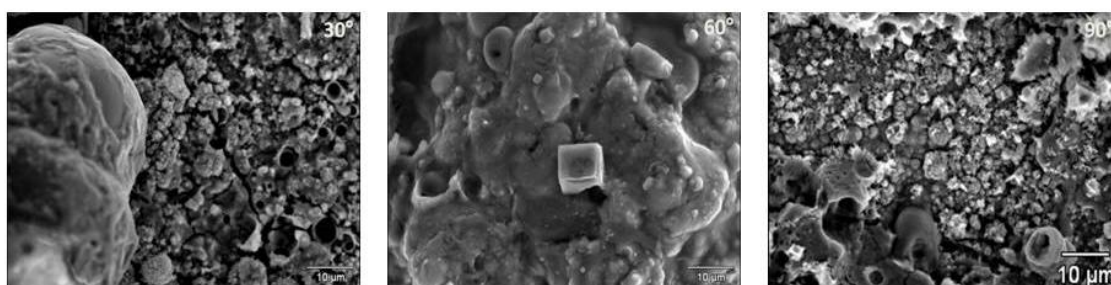


Figure 11. Micrographs of corrosion products deposited on the metallic coupons at the impingement angles indicated and a flow rate of 18 L/min

Corrosion products in Figure 11 are classified within the toothed type in a porous surface, which is more evident for coupons at 30° and 90°; while on the surface of the coupon placed at 60° a relative greater amount of deposits is observed. The corrosion products formed displayed an increase in the density of agglomerates as the impact angle was increased from 30 to 90°. In the three surfaces, the growth of corrosion products is observed to be developed in layers, this behavior can be better observed in the coupon at 90°. The removal of corrosion products is not only derived from the flow effect on surface but also from the nature of crystalline layers, which are more or less susceptible to cracking.

3.4 XRD Characterization of corrosion products

To characterize the corrosion products in the samples of API 5L X-70 steel, immersion tests were carried out in the testing environment for 24 hours.

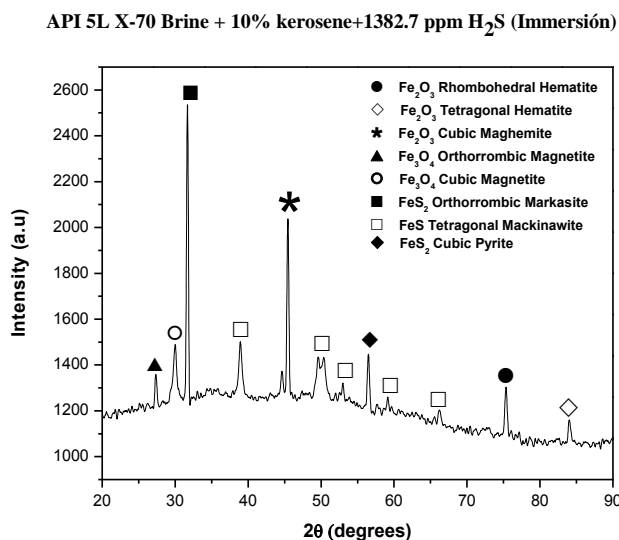
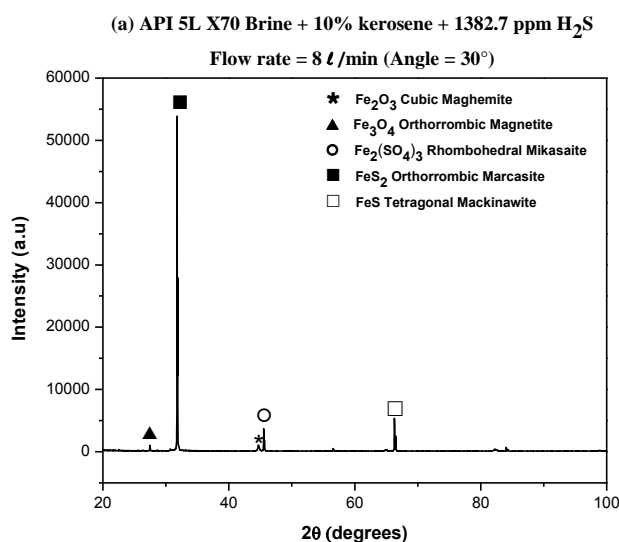


Figure 12. XRD analysis of corrosion products in API 5L X-70 after immersion tests for 24 hours in sour brine.

Figure 12 shows the diffraction pattern in static condition with the feature that sulfides predominated over oxides. The presence of mackinawite (FeS) as a base precursor [15] and the growth of layers of corrosion products is observed. Layers consisted of rhombohedral hematite (Fe₂O₃), tetragonal hematite (Fe₂O₃), cubic maghemite (γ-Fe₂O₃), orthorhombic magnetite (Fe₃O₄), cubic magnetite (Fe₃O₄), orthorhombic marcasite (FeS₂) and cubic pyrite (FeS₂). These products are equivalent to the iron sulfides reported by Ning *et al.* [15], where it is emphasized the importance of polymorphism of crystalline phases on film mechanical properties, which coincided with the identification made by Cervantes *et al.* [16].



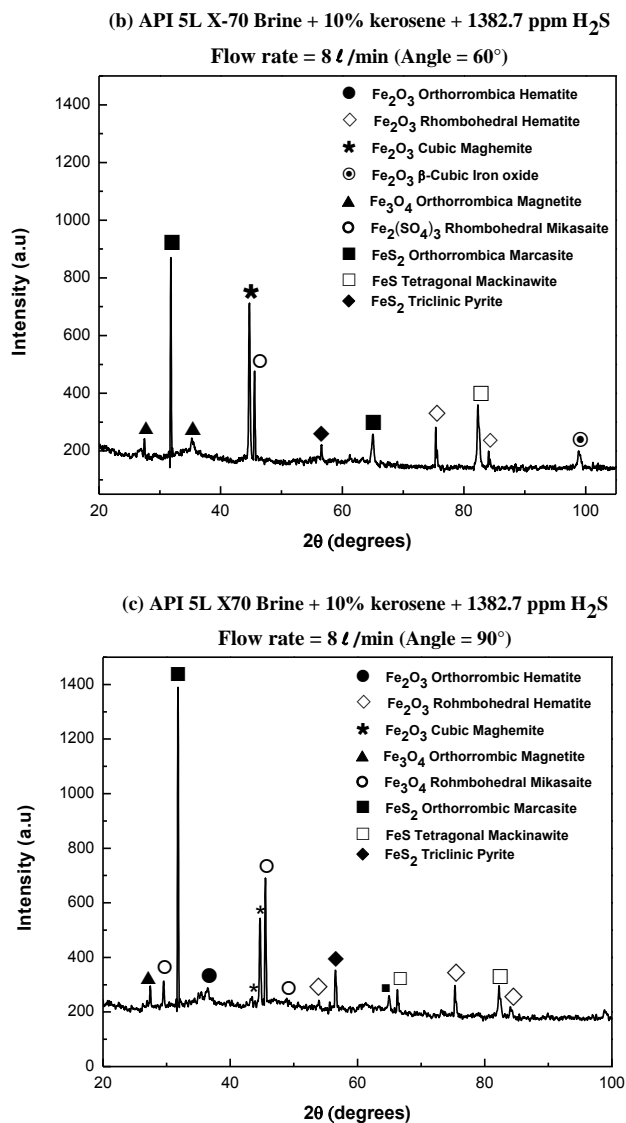


Figure 13. X-ray diffraction analysis (XRD) of corrosion products in API 5L X-70 steel surface in sour brine (a) 30°, (b) 60° and (c) 90° and flow rate of 8 L/min.

Figure 13 shows the diffraction patterns obtained for the coupons under the test conditions at a flow rate of 8 L/min (1.05 m/s) at 30, 60 and 90°, respectively. The phases presented for the three angles are tetragonal mackinawite (FeS), orthorrombic magnetite (Fe₃O₄), cubic maghemite (Fe₂O₃), orthorrombic marcasite (FeS₂) and iron sulfate, known as rhombohedral mikasaite (Fe₂ (SO₄)₃). Qualitatively sulfides predominated over oxides for the three-impingement angles; with the additional feature, that triclinic pyrite (FeS₂) is observed at 60° and 90°. Orthorrombic marcasite (FeS₂) was the predominant phase appearing on the surfaces subjected to the three impingement angles. This face appeared where the corrosion products grew and it is assumed that aided in the mitigation of corrosion [17].

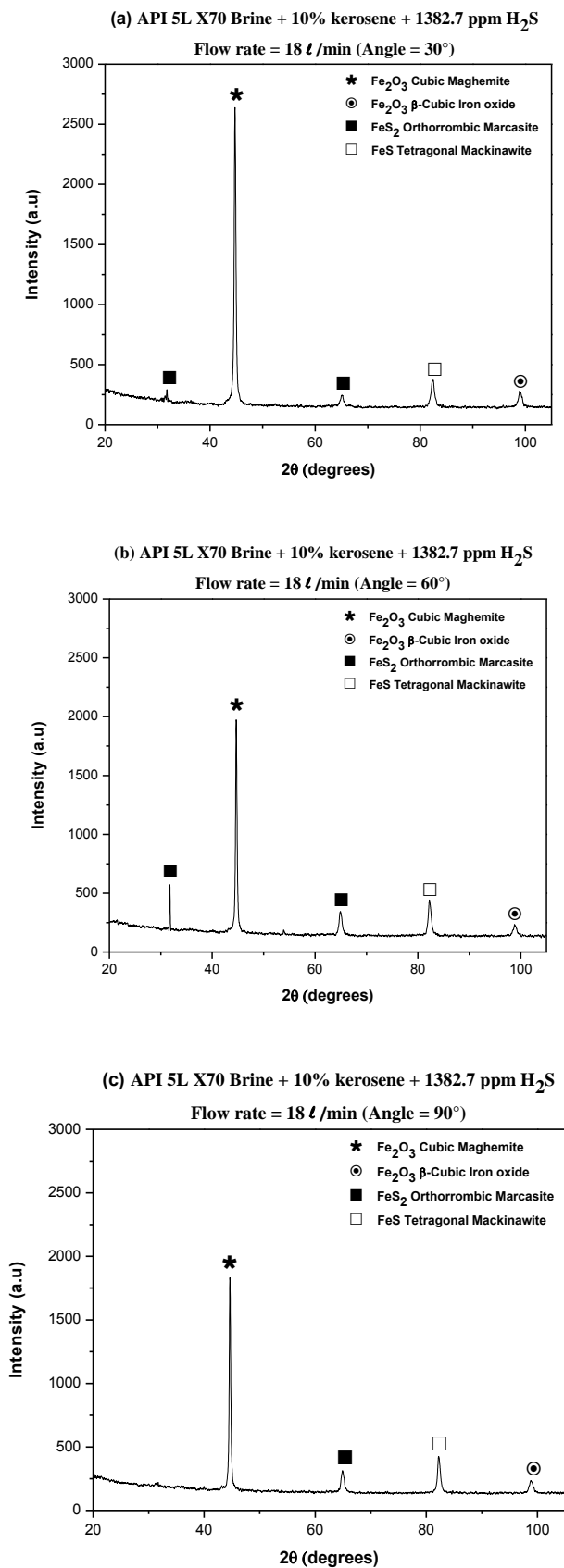


Figure 14. X-ray diffraction analysis (XRD) of corrosion products in API 5L X-70 steel surface in sour brine at (a) 30°, (b) 60° and (c) 90° and a flow rate of 18 L/min.

The phases that appeared in the diffraction patterns at a flow rate of 18 L/min are basically the same for the three angles of impingement: tetragonal mackinawite (FeS), cubic maghemite (Fe₂O₃), orthorhombic marcasite (FeS₂) and β -cubic iron oxide (Fe₂O₃). The presence of marcasite might explain the low corrosion rates at the angles of inclination of 30°-90°, as it is known as a stable corrosion product that contributed to decrease corrosion rate because the adherence of crystal lattice on steel surface [17]. The cubic maghemite shows a decrease in its peak as the angle increased, just as it did the iron oxide-cubic β , while marcasite displayed two peaks (30°, 60°) but only one at 90°. In this case, the corrosion products formed are the same, with the feature that now oxides predominated over sulfides; it appears that the high flow rate allowed only the formation of a lower number of phases though of high stability as fluid rate did not provide sufficient time for chemical reaction to occur.

4. CONCLUSIONS

The distribution, morphology and growth of corrosion products formed on pipe steel in sour brine suggested that the corrosion process occurred by the formation of consecutive film layers, which seems to be deposited randomly one on the other as detected by microscopy. It appears that marcasite (FeS₂) and maghemite (Fe₂O₃) predominated under static conditions forming more sulfides. At 8 L/min, the formation of sulfides prevailed to form marcasite (30°); marcasite and maghemite (60°); marcasite and (Fe₃O₄) micasaite (90°). In contrast, at 18 L/min, cubic maghemite (Fe₂O₃) predominated at each impingement angle to favor the formation of oxides. In the latter case, the flow rate of 18 L/min led to higher corrosion rates and suggested that oxides films are less corrosion and strength resistant than sulfides. Likewise, immersion test yielded eight different compounds on film, while at 18 L/min only four compounds were formed so flow rate decreased the number of crystalline phases and increased corrosion rate.

The highest corrosion rates were displayed at 90° at 8 L/min (90, 120 mpy) and 18 L/min (200 mpy); it is thought that flow direction might induce normal stresses higher than those shear stresses formed at lower angles (30°, 60°). This indication is assumed to be associated to an easier process of corrosion product detachment due to stress level and physico-chemical properties of deposited phases, though this remained to be proved.

ACKNOWLEDGEMENTS

The authors would like to thank The Consejo Nacional de Ciencia y Tecnología (CONACYT), the Instituto Politécnico Nacional (IPN) and the Grupo de Análisis e Integridad de Ductos (GAID) for the grant awarded to Mr. Galván-Luis. Acknowledgments are also due to the Instituto Mexicano del Petróleo for partial sponsorship.

References

1. S. Nasrazadani, R.K. Nakka, D. Hopkins, J. Stevens, *International Journal of Pressure Vessel and Piping*, 86 (2005) 845-852.
2. V.K. Chexal, J. Horowitz, RB Dooley, *EPRI TR-106611R1*, July 1998.

3. R.B. Dooley, V.K. Chexal, *International Journal of Pressure Vessels and Piping*, 77 (2000) 85-90.
4. J. M. Pietralik, *E-Journal of Advanced Maintenance (EJAM)*, Vol.4, No.2 (2012) 63-78.
5. Li Xiao-yan, Lü Tao, *Technol. Journal*, Vol. 12 (2005) 119-123.
6. K. Vivekanand, S. Roychowdhury, P. Ahmedabadi, D.K. Barua, *Engineering Failure Analysis*, Vol. 18 (2011) 2028-2041.
7. S. Paul, *J. Materials Engineering and Performance* 20 (2011), 325-334.
8. R. Kern, *Chemical engineering* 23 (1974), 58-66.
9. NACE 1D-196: "Laboratory Test Methods for Evaluating Oilfield Corrosion Inhibitors" (Houston TX: NACE, 1996).
10. ASTM G59-97 (Reapproved 2003), "Standard Test Method for Conducting Potentiodynamic Polarization Resistance Measurements". ASTM G102-89 (Reapproved 2010), Calculation of corrosion rates and related information from electrochemical measurements. ASTM international, West Conshohocken PA, United States.
11. R. Dong, I. Sun, Z. Liu, X. Wang and Q. Liu, *Journal of Iron and Steel Research International*, 15 (2008) 71.
12. D. Clover, B. Kinsella, B. Pejicic and R. De Marco, *Journal of Applied Electrochemistry*, 35 (2005) 139.
13. C.W. Du, X.G. Li, P. Liang, Z.Y. Liu, G.F. Jia and Y.F. Cheng, *Journal of Materials Engineering and Performance*, 18 (2009) 216.
14. D. Ricard, G. Luther, *Chemical Reviews*, 107 (2007) 514-562.
15. J. Ning, Y. Zheng, D. Young, B. Brown, S. Nesic, A Thermodynamic Study of Hydrogen Sulfide Corrosion of Mild Steel, NACE international, 2013, paper 2462.
16. A. Cervantes-Tobón, M. Díaz-Cruz, J.L. González-Velázquez, J.G. Godínez-Salcedo, *Int. J. Electrochem. Sci.*, 9 (2014) 2254-2265.
17. J.S. Smith, J.D.A. Miller, *Corrosion Journal*, 10(3) (1975) 136.

© 2015 The Authors. Published by ESG (www.electrochemsci.org). This article is an open access article distributed under the terms and conditions of the Creative Commons Attribution license (<http://creativecommons.org/licenses/by/4.0/>).